

We are IntechOpen, the world's leading publisher of Open Access books Built by scientists, for scientists

6,900

Open access books available

186,000

International authors and editors

200M

Downloads

Our authors are among the

154

Countries delivered to

TOP 1%

most cited scientists

12.2%

Contributors from top 500 universities



WEB OF SCIENCE™

Selection of our books indexed in the Book Citation Index
in Web of Science™ Core Collection (BKCI)

Interested in publishing with us?
Contact book.department@intechopen.com

Numbers displayed above are based on latest data collected.
For more information visit www.intechopen.com



Application of Nanoimprint Lithography to Distributed Feedback Laser Diodes

Masaki Yanagisawa
Sumitomo Electric Industries, Ltd.
Japan

1. Introduction

The recent growth of information-communication facilities such as the Internet, mobile telecommunication and video-on-demand services has led to explosion of worldwide communication traffic, which increase demand for faster and denser communication infrastructures including optical communication networks. Distributed feedback laser diodes (DFB LDs) have been widely used as optical sources in networks because of their high selectivity and stability of wavelength. Although they had limitedly been used in long-haul and high-speed network at one time, they are now increasingly required in metro and end-user fields because of the increasing traffic. Thus, necessity for inexpensive DFB LDs increases rapidly.

The characteristics of a DFB LD with uniform (constant period) gratings depend on the grating phase at the cleaved facet (Matsuoka et al., 1984). The variation of characteristics with the facet phase is a serious issue in view of productivity and usability of the LDs. One of the most effective ways of reducing the facet phase effect is to adopt phase-shifted gratings instead of uniform gratings (Kaden et al., 1992). The uniformities of the LD characteristics such as mode-stability and output power are improved by adopting phase-shifted gratings, thus the yield of LDs increase and their production cost is effectively reduced.

In general, there are various fabrication methods for diffraction gratings of DFB LDs, for example, interference exposure, electron beam lithography (EBL), and optical projection exposure. Interference exposure cannot feasibly be used for fabricating phase-shifted gratings, because it exclusively generates exposure patterns with a uniform bright-and-dark period. Although EBL has sufficient resolution to be used for phase-shifted gratings, exceedingly expensive apparatus is necessary for volume production with sufficient throughput. For the optical projection method, a forefront stepper having sufficient resolution for gratings is also expensive, and the cost is too high for fabricating DFB LDs, of which production volume is relatively small compared to that of such semiconductor devices as LSIs.

Nanoimprint lithography (NIL) has been studied by many organizations since the middle of the 1990s. Chou et al. indicated that sub-10-nm features could be formed by imprint, which started the era of NIL technology (Chou et al., 1995). A novel method of NIL using a UV-curable resin was introduced by Haisma et al (Haisma et al., 1996), and Bailey et al.

demonstrated a step-and-repeat imprint method named SFIL (Bailey et al., 2000). NIL is a simple method applicable to forming fine patterns smaller than 100 nanometers, so it is studied as a candidate for a next-generation fabrication technique in many application fields such as storage devices, displays, optical devices, MEMS, semiconductor and so on.

Since 2004, we have investigated the use of NIL for fabricating diffraction gratings, because the new technology have been considered as an attractive solution to the above issues concerning the fabrication of phase-shifted gratings because of its high resolution, throughput, and low cost. In 2009, we have reported that our NIL method have been successfully applied to fabricating quarter-wavelength shifted DFB LDs (Yanagisawa et al., 2009). To the best of our knowledge, it is the unprecedented demonstration of NIL application to DFB LDs in wafer-scale fabrication having the potential of near-future volume production.

2. Fabrication process

Our fabrication method is based on our conventional production process of DFB LDs except for the formation of diffraction gratings by NIL, which is a strong point because we make the best use of the mature process and minimize the risk of unpredictable difficulties induced by adopting new methods.

From an early stage of this study, we have used UV-NIL rather than other imprint methods such as thermal NIL and soft lithography, because UV-NIL has advantages of high over-layer alignment accuracy, low imprint pressure and high throughput. Over-layer alignment is especially important in view of mixing and matching the NIL method with the conventional LD fabrication. Imprint pressure is desirable as low as possible, because it directly influences crystal damage of a substrate as described later.

2.1 Mold design

One of the major issues of applying NIL process to DFB LDs is preparation of molds (templates). In general, NIL molds are fabricated by utilizing the forefront method such as electron-beam lithography (EBL), whose throughput is much lower than other optical lithography methods. Thus, long delivery time and high cost for mold fabrication are serious problems. DFB LDs generally used in optical networks vary in emission wavelengths from 1.3 μm to 1.6 μm , thus corresponding periods of diffraction gratings accordingly vary from 200 nm to 250 nm. If a mold were designed with containing the sole type of grating period, we would have to prepare a large number of molds for covering all wavelength range. It would lead to insurmountably high initial costs for DFB LD fabrication.

We have developed a novel NIL method with a new concept of mold design named "VARI-mold." In the new process, one mold can be used for fabricating various types of DFB LDs with different wavelengths. The prepared mold contains more than 9000 grating patterns in an imprint field, consisting of about 900 subfields, and each subfield contains more than 10 different types of grating patterns with the period from 194 nm to 248 nm exemplified in Fig. 1. As described in the next section, various types of LDs are fabricated by utilizing one VARI-mold, leading to reducing the cost for mold preparation.

The molds used in this study are fabricated by a reticle fabrication method and an etching procedure.

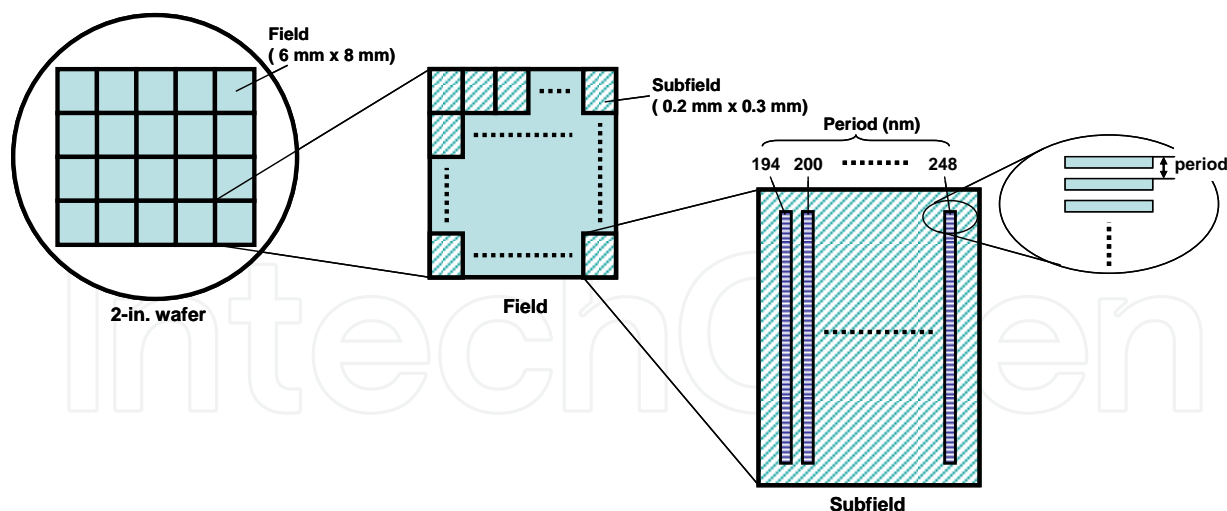


Fig. 1. Schematic structure of a "VARI-mold"

2.2 Wafer fabrication

In general, commercially available compound semiconductor substrates used for optical devices, such as GaAs, InP, and GaN, have large undulations compared with Si substrates widely used for electronic devices such as LSIs and memories. For example, 2-in. diameter InP substrates, which are generally used for fabricating DFB LDs, typically have over $3\ \mu\text{m}$ in total thickness variation. If such undulating substrates are applied to NIL, the mold probably come in contact with a limited portion of the substrate, in which case severe nonuniformity of the residual layer thickness will lead to large variations of the transferred figures in the imprinted area. Thus, we have formed diffraction gratings by using a reverse-tone nanoimprint in order to suppress the variation of residual layer thickness resulting from the undulation of substrates (Miller et al., 2005).

A schematic structure and a layer structure of the LD are shown in Fig. 2. We have prepared a 2-in. InP wafer with epitaxial layers including a grating layer, an active layer, a buffer layer and a lower cladding layer grown by metalorganic vapor phase epitaxy (MOVPE).

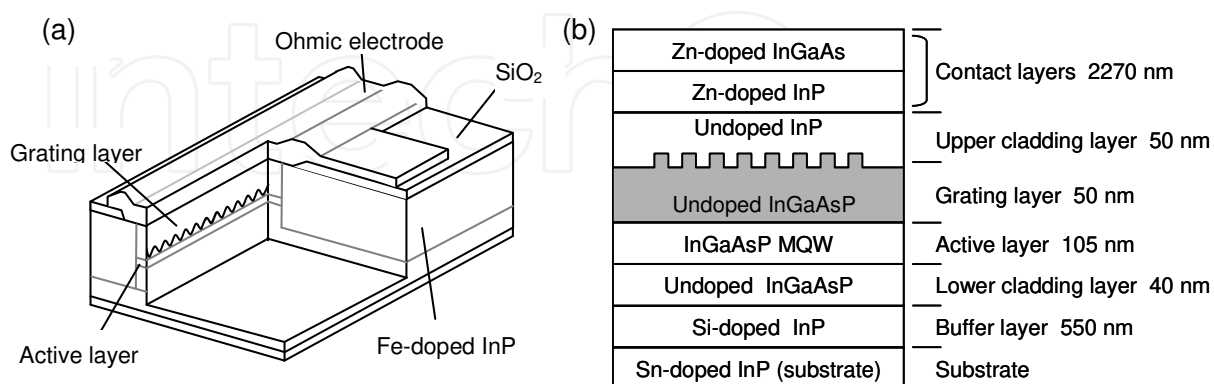


Fig. 2. Schematic structure of a DFB LD (a) and crystal layer structure of the prepared wafer (b).

The fabrication procedure is shown in Fig. 3. First, a 50-nm-thick SiN film is deposited on the wafer by plasma-enhanced chemical vapor deposition (PE-CVD). Next, a primer

material is spin-coated in order to increase adhesion between UV-curable resin and the SiN film. Then, UV-NIL using a VARI-mold is conducted to form grating patterns in the UV-curable resin layer (Figs. 3(a) and 3(b)). In this study, imprinting was performed in 16 fields on the wafer with a step-and-repeat equipment. The imprint pressure before UV exposure is approximately 0.1 MPa, and the exposure time is 20 seconds. After the imprint, Si-containing resin is spin-coated in order to cover and planarize the grating corrugations (Fig. 3(c)). The thickness of the planarization layer is approximately 200 nm. Subsequently, the planarization layer is etched by reactive ion etching (RIE) until the tops of the corrugations are revealed (Fig. 3(d)). After that, the revealed layer is selectively etched and penetrated until the SiN masks are revealed (Fig. 3(e)). This penetration etching is one of the essential techniques of this process, so detailed in next section. The formed resin patterns are used as masks for the subsequent etching, transferring the grating patterns to the SiN film (Fig. 3(f)). Next, the resin layers are removed by O₂ plasma etching. After that, we use inductively coupled plasma RIE (ICP-RIE) with CH₄ / H₂ gas for etching of the crystal layer (Fig. 3(g)). Finally, the SiN masks are stripped by a wet chemical process using HF solution, and the diffraction grating structure is achieved. After the formation of the gratings, an upper cladding layer and contact layers are formed on the grating layer by MOVPE. The contact layers consist of InP and InGaAs layers. Then, stripe patterns of SiO₂ are formed on the contact layer by using chemical vapor deposition (CVD) and conventional photolithography method in order to define the cavities of the DFB LDs. In this step, cavity stripes are overlaid to the grating patterns having a specific period corresponding to the required wavelength of LDs. For example, when we would fabricate DFB LDs with the wavelength of 1310 nm, stripe patterns had to be aligned onto 200 nm-period gratings (Fig. 4). As a matter of course, different types of LDs with various wavelengths can be achieved simultaneously on a wafer provided that we adjust the alignment of the cavity stripe layer in each imprint field. The stripe patterns of SiO₂ are used as masks for subsequent crystal etching by ICP-RIE with CH₄ / H₂ gas. In this etching step, all unused grating patterns (excepting the selected one under the stripe) are removed. After that, Fe-doped InP is selectively grown onto the etched area as an insulating layer by MOVPE. Subsequently, a SiO₂ film is deposited as a passivation layer, in which contact holes are formed by selective etching by RIE. Finally, metal electrodes are formed by high-vacuum evaporation and a lift-off method.

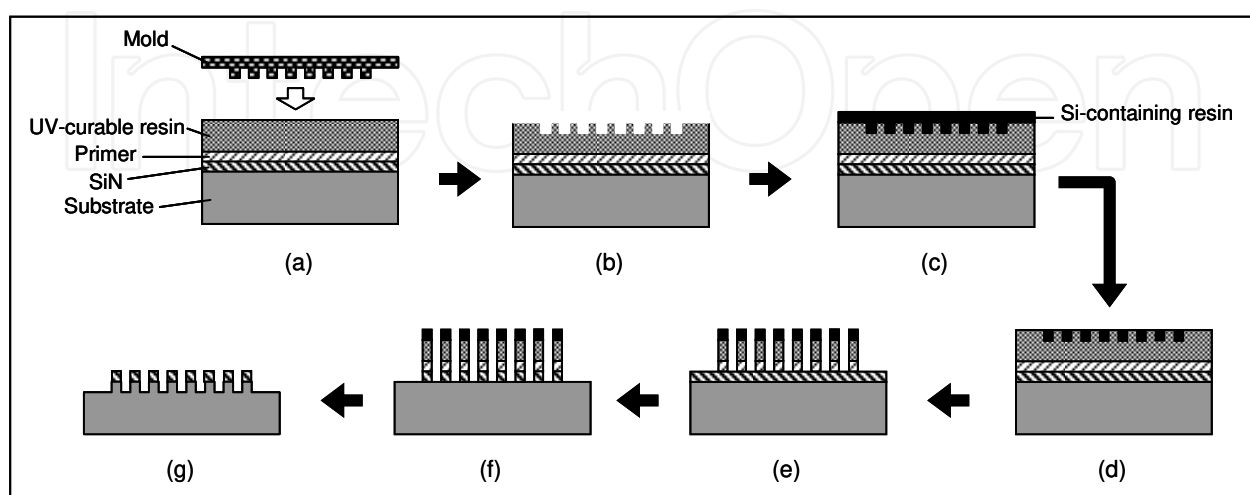


Fig. 3. Fabrication process of diffraction gratings.

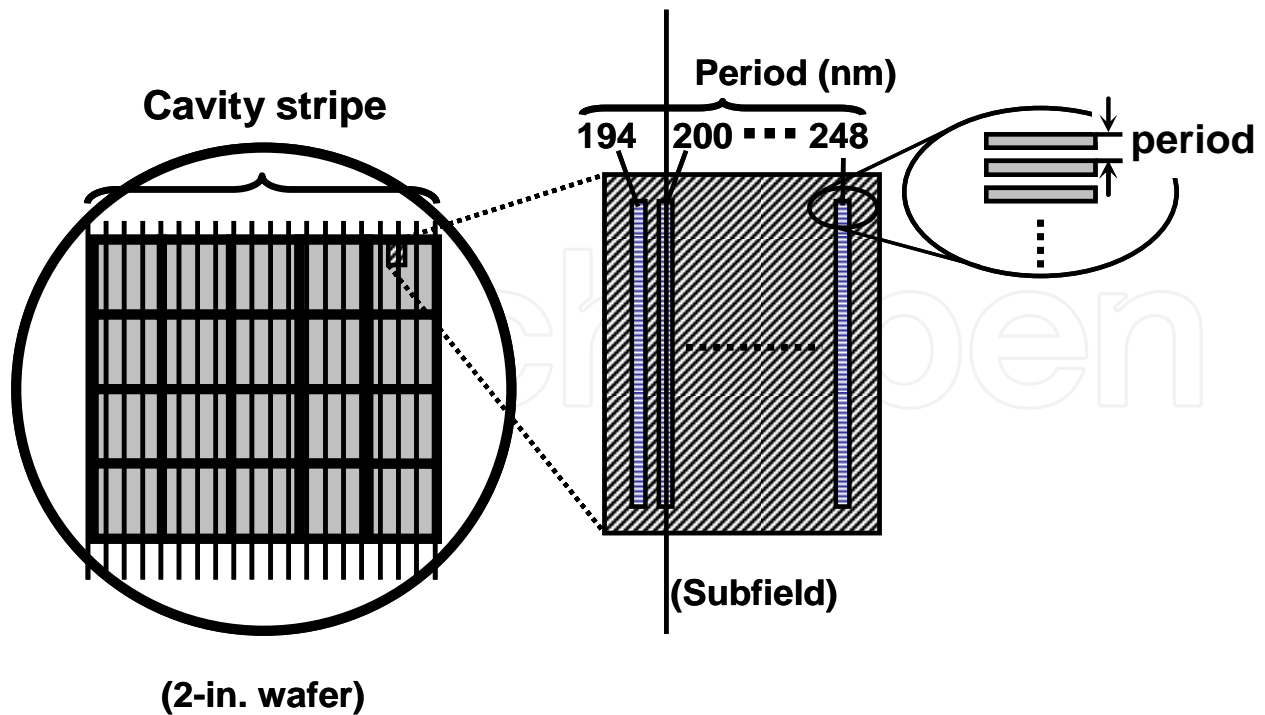


Fig. 4. Concept of cavity stripe delineation.

2.3 Etching process

As mentioned above, the resin etching is one of the key techniques of our fabrication process. Nonuniformity of the linewidth of corrugations after the penetration etching leads to inhomogeneity of the grating figures (Fig. 3(e)), resulting in yield reduction of DFB LDs.

We have developed the etching method using a low-temperature ICP-RIE system in order to achieve highly-uniform and highly-repeatable grating fabrication (Tsuji et al., 2011). The etching method is characterized by the etching gas and the low-temperature substrate stage. Oxygen and nitrogen are used as the etching gas, and the substrate stage is controlled with the temperature from 260 K to 270 K. The both features contributes to suppress the undercut of the UV-curable resin during the penetration etching, resulting from the sidewall effect produced by the optimized plasma condition and substrate temperature (Kure et al., 1991; Kinoshita et al., 1999). The optimized etching condition is shown in Table 1, and a cross-sectional view of the grating after the penetration etching observed by a scanning electron microscope (SEM) is shown in Fig. 5.

Gas flow rate	N ₂	9 sccm
	O ₂	1 sccm
Bias power		70 W
ICP power		250 W
Substrate temperature		263 K

Table 1. Etching condition of the penetration etching.

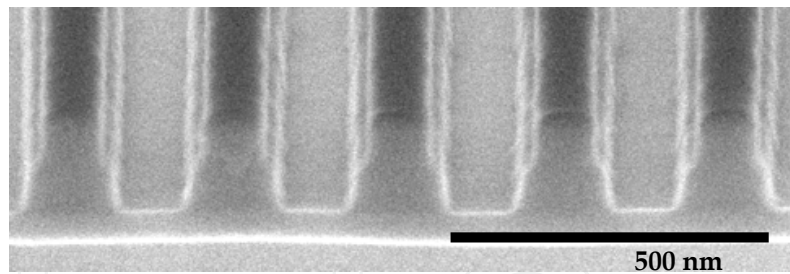


Fig. 5. SEM image of the diffraction grating after the penetration etching.

We have evaluated the linewidth uniformity of the corrugations within 6 wafers. Figure 6 is the histogram of the linewidth, indicating the standard deviation is less than 4 nm.

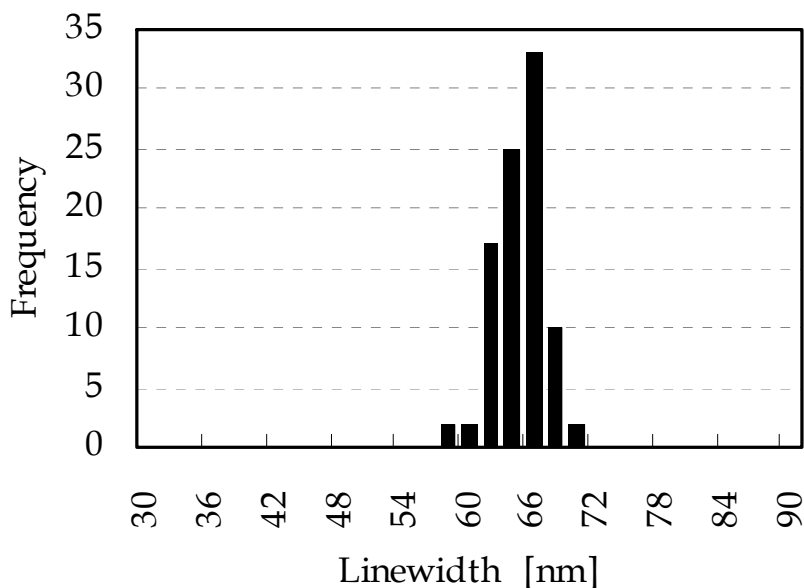


Fig. 6. Histogram of the corrugation linewidth within 6 wafers after the penetration etching.

3. Results

When we use NIL for fabricating DFB LDs, we have paid attention to mechanical damage in epitaxial layers by imprint pressure, because compound semiconductor crystals used for LDs are easily damaged by mechanical stress, leading to severe deterioration in long-term reliability of device characteristics (Fukuda et al., 1985). In this study, photoluminescence (PL) method have been used for evaluation of the crystal damage, and simple 2-D simulation is conducted as qualitative analysis of distribution of the PL intensity.

Furthermore, we have also focused on the accuracy of the grating period, because it dominantly influences the emission wavelength which is the essential parameter of LD characteristics. The emission wavelength directly impacts on the yield of DFB LDs, so its repeatability is required to be sufficiently high for volume production. We have verified the accuracy of the grating period by measuring diffraction angles described below.

Finally, we have fabricated quarter-wavelength shifted DFB LDs by utilizing the new fabrication process combining NIL and the conventional LD process, and evaluated their characteristics including long-term reliability.

3.1 Influence of imprint pressure

3.1.1 Photoluminescence intensity

In order to evaluate the mechanical damage in semiconductor crystal induced by imprinting pressure, we have investigated deterioration of PL intensities from the epitaxial layers. We prepared two indium-phosphide substrates with epitaxial layers and a blank (with no patterns) mold. We compared photoluminescence intensities between the two samples: imprinted with UV-curable resin between the mold and the substrate, and imprinted without resin. The field size of the blank mold used here is 10 mm x 10 mm. The evaluation results of PL intensities are shown in Fig. 7. Field size of the blank mold used here is 10 mm x 10 mm. Imprinting pressure is 0.8 MPa for both samples. The sample without resin shows evident deterioration of PL intensities indicated in dark (green-like) colors in Fig. 7. The deteriorations of intensity are found mainly in the edge of the imprinted area. This means that the imprinting pressure concentrates near the edge of the mold. On the other hand, no evident deterioration is found in the sample with resin. These results indicate that the resin functions such as a cushion to prevent severe damage in epitaxial layers by imprinting pressure.

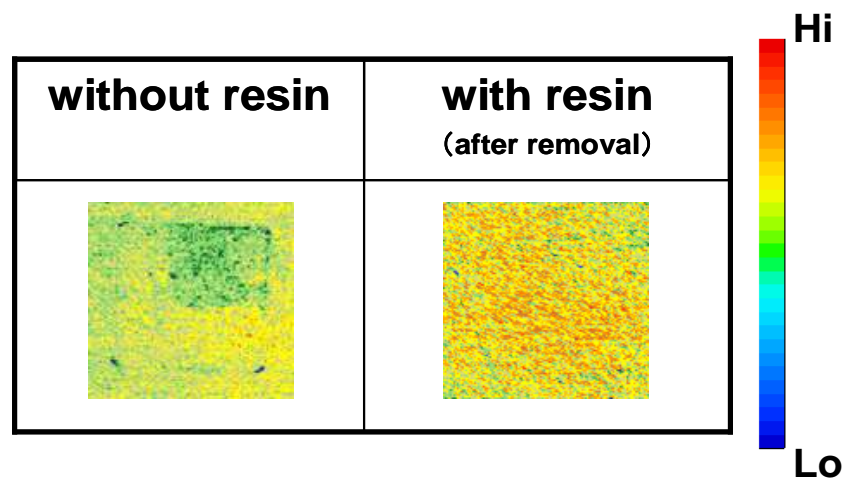


Fig. 7. PL intensities of the epitaxial layers after imprints. The field size of the imprint is 10 mm x 10 mm.

3.1.2 Simulation

We have calculated how resin between a mold and a substrate influences on mechanical stress induced in the substrate. We used a simple model for the finite element method (FEM) as described in Table 2 and Fig. 8. In this study, UV-curable resin is to be considered as liquid having nonlinear viscoelasticity; however, elastomer is substituted for resin because we do not have an adequate tool for dynamic simulation of viscoelastic material. Thickness and the Young's modulus of the elastomer are assumed of 50 nm and 1000 MPa, respectively. Imprinting pressure is 1×10^7 MPa. The elastomer and the other materials are connected with common FEM nodes at the boundaries.

Figure 8 shows two-dimensional distribution of von Mises stress in molds and substrates. For the sample without elastomer, mechanical stress is concentrated in periphery of the edge of the mold [Fig. 8(a)]. On the other hand, when the elastomer is supposed between the mold and the substrate, concentration of stress on the surface of the substrate is clearly suppressed [Fig. 8(b)]. These results are qualitatively consistent with the evaluation using PL described in above section.

		Young's modulus [MPa]	Poisson ratio
Mold	SiO ₂	70000	0.17
Substrate	InP	60700	0.36
Liquid	Elastomer	1000	0.49

Table 2. Mechanical properties used for the stress simulation.

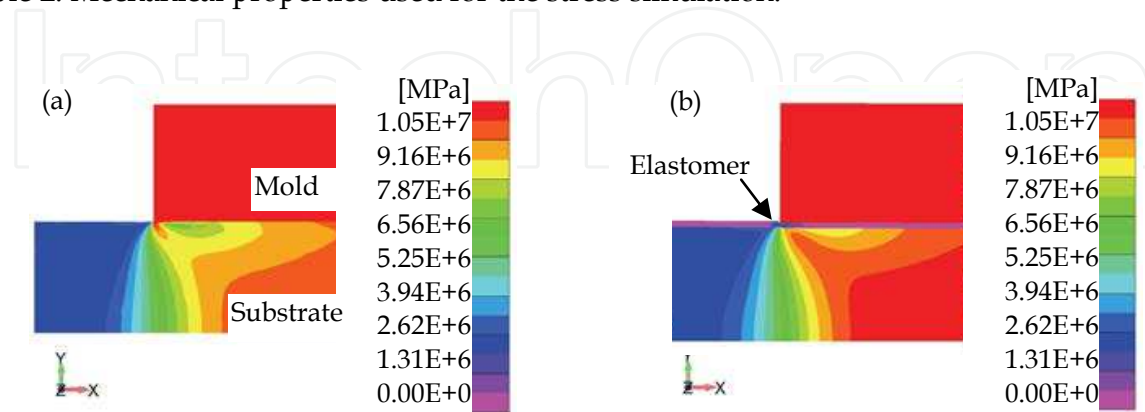


Fig. 8. Distribution of von Mises stress without (a) and with (b) elastomer between a mold and a substrate.

3.2 Grating figure

A SEM image of the fabricated diffraction gratings is shown in Fig. 9. It demonstrates that the line edge roughness (LER) of the gratings is markedly low, indicating that the LER of the grating corrugations in the master mold is sufficiently suppressed and that the master patterns are precisely transferred to the substrate by the imprinting and the subsequent etching process. The depth of the diffraction gratings was measured to be approximately 15 nm by an atomic force microscope.

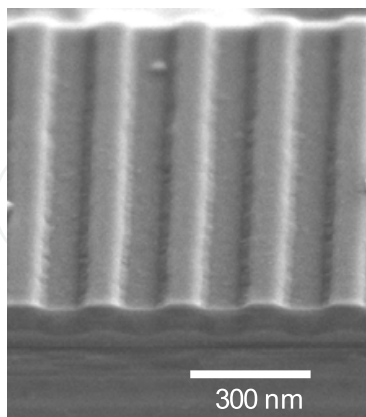


Fig. 9. SEM image of diffraction gratings.

3.3 Reproducibility of the grating period

The diffraction gratings with the period from 194 to 204 nm have been formed on a 2-in. InP wafer. The grating periods have been verified by measuring the diffraction angles of the transferred grating patterns. The wavelength of the incident light is 364.8 nm, and the

measurement error of the grating period is estimated less than 0.03 nm. Figure 10 shows a correlation between the grating periods of the mold and those of the transferred patterns. The difference between both of the values is less than 1%, and the wafer-to-wafer variation of the periods is less than 0.2 nm through the 6 wafers. This shows that the NIL process has high reproducibility in transferring grating patterns.

3.4 Device characteristics

We have evaluated DFB LDs fabricated by our novel process in order to verify the basic characteristics and their uniformity in 2-in. wafer. The nominal wavelength of the measured LDs is 1490 nm, and the corresponding grating period is approximately 232 nm (excluding Fig. 12).

Figure 11 shows the dependence of the optical output and the slope efficiency on the supplied current for a typical phase-shifted DFB LD fabricated in this study. The threshold current and the slope efficiency at room temperature were measured to be 8 mA and 0.28 W/A, respectively, which are comparable to those of typical phase-shifted DFB LDs fabricated by utilizing the conventional EBL process.

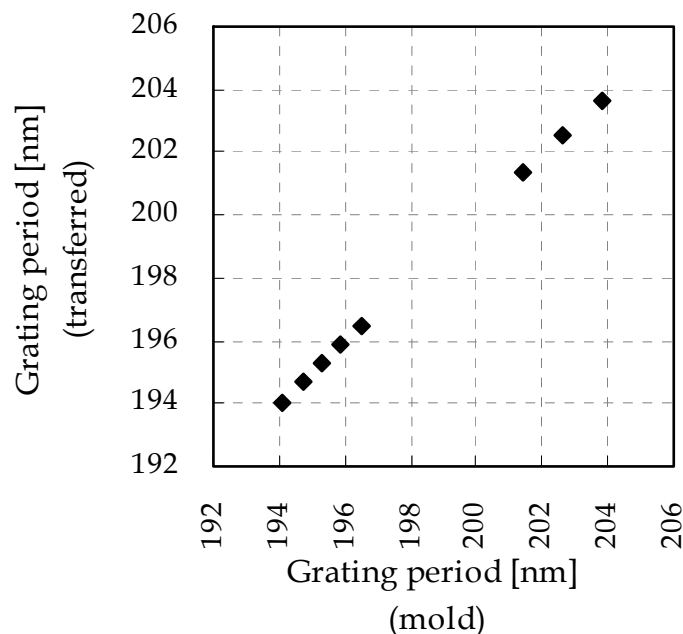


Fig. 10. Correlation between the designed (horizontal) and the measured (vertical) grating periods.

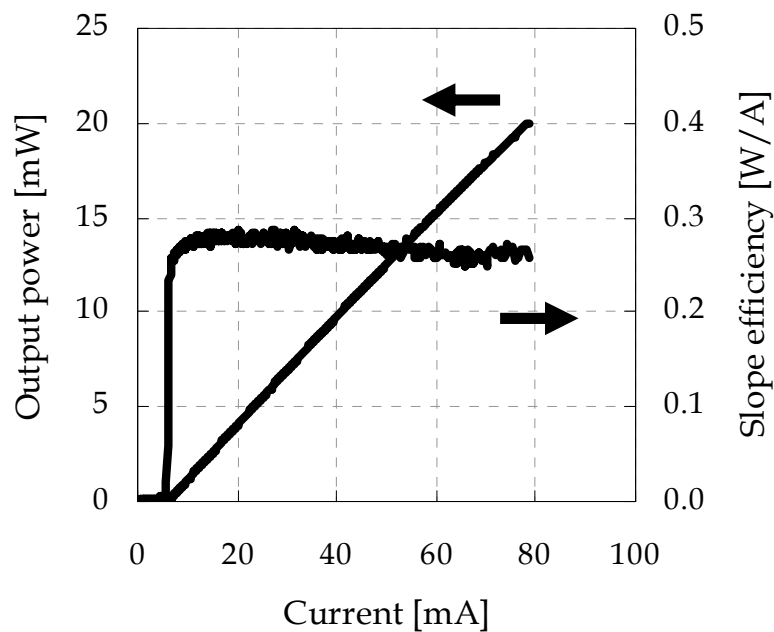


Fig. 11. Supplied current vs optical output and slope efficiency.

Figure 12 shows the oscillation spectrum of a phase-shifted DFB LD. The resolution of the wavelength is 0.02 nm. This demonstrates that the peak wavelength corresponds to the Bragg wavelength at the center of the stopband, indicating that the phase-shifted gratings function properly.

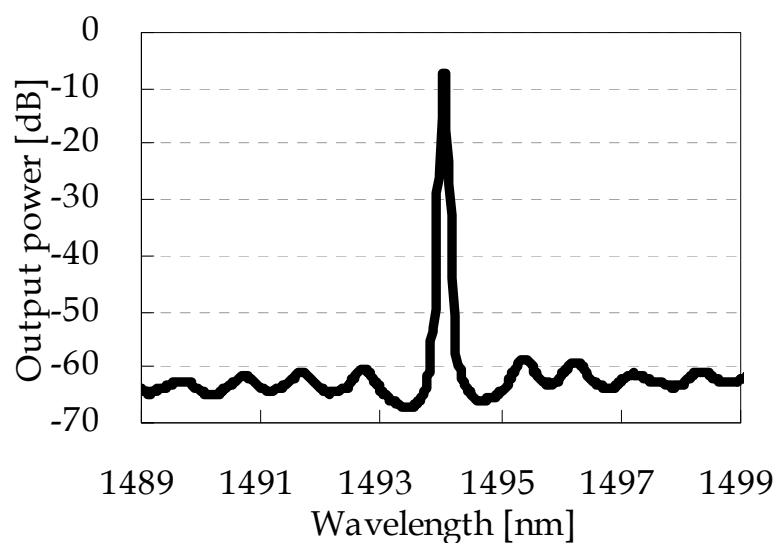


Fig. 12. Oscillation spectrum of the DFB LD.

Figure 13 shows the oscillation spectra of DFB LDs with the grating period of 195 nm and 202 nm, which are simultaneously fabricated on a wafer. This demonstrates that the peak wavelengths correspond to the respective Bragg wavelengths corresponding to each grating period.

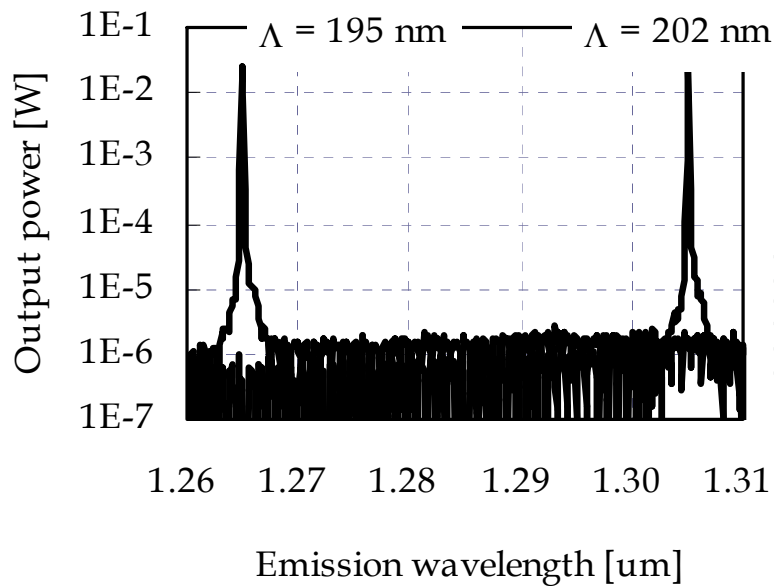


Fig. 13. Oscillation spectra of the DFB LDs with the grating period (Λ) of 195 nm and 202 nm.

We have compared the side-mode suppression ratio (SMSR) of phase-shifted LDs fabricated by NIL with those fabricated by EBL. SMSR is one of the parameters indicating the stability of the single-mode emission of DFB LDs. More than 300 LDs randomly sampled from respective 2-in. wafers have been evaluated. Histograms of SMSR for both types of LD are shown in Fig. 14, which demonstrate that they show comparable variations in SMSR.

These results indicate that DFB LDs fabricated here by utilizing NIL have comparable characteristics and their uniformities to ones by conventional EBL process.

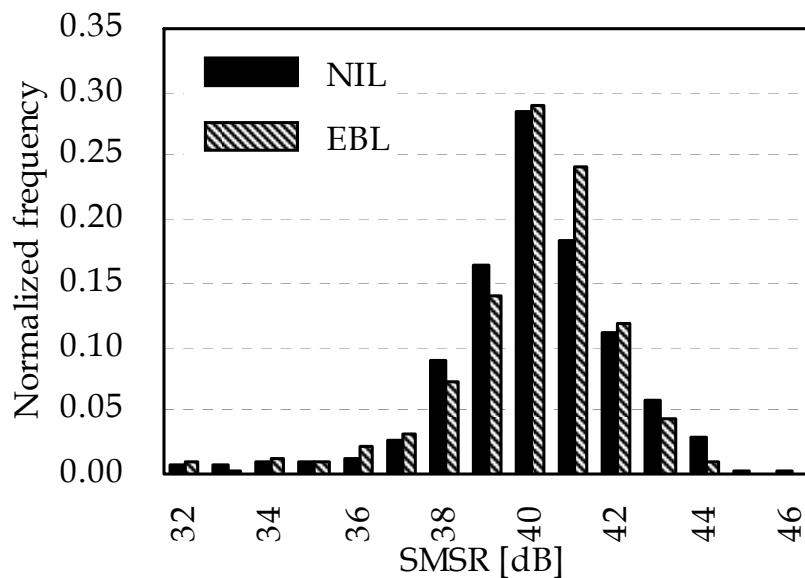


Fig. 14. Histograms of SMSR for phase-shifted LDs fabricated by NIL and by EBL. The standard deviations of SMSR are almost the same, 2.0 and 1.8, respectively.

3.5 Reliability

We have investigated long-term reliability of fabricated DFB LDs. Figure 15 shows the time-dependent change in the threshold current of phase-shifted LDs with the output power of 10 mW at the ambient temperature of 358 K. The number of samples is 18. The change in the threshold current after 5000 hours is less than $\pm 1\%$, indicating that the phase-shifted DFB LDs fabricated in this study have high stability in lasing characteristics.

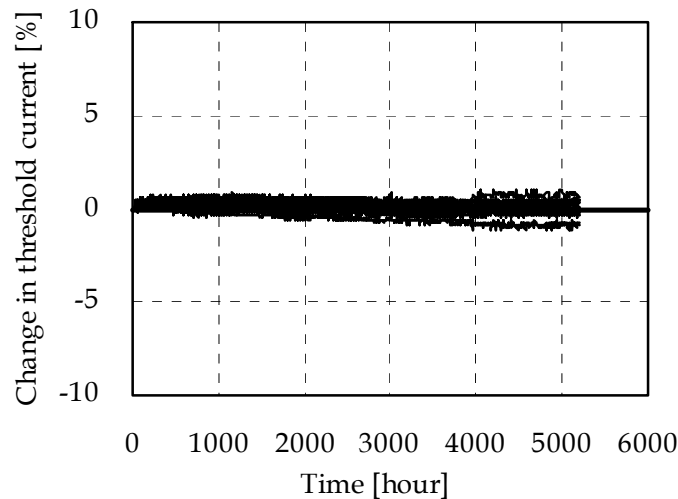


Fig. 15. Time-dependent change in the operation current of the DFB LDs with the output power of 10 mW at the ambient temperature of 358 K.

4. Conclusion

We have successfully demonstrated fabrication of phase-shifted DFB LDs by utilizing NIL process, which have comparable characteristics and their uniformities to ones fabricated by conventional EBL process. Fabricated DFB LDs have shown high stability of characteristics in long-term reliability test. We have also demonstrated the feasibility of the VARI-mold, which can be used for the fabrication of DFB LDs with various wavelengths, indicating that we can drastically reduce the cost of molds in our mass production phase in the near future. Considering the results above, we conclude that NIL is a promising candidate of the production technique for phase-shifted DFB LDs featuring low cost and high throughput.

NIL is expected to be used as a fabrication process for many applications. However, there are still some difficulties with its use as a mass-production process, for example, defects and low throughput in patterned media, defects and poor alignment accuracy in semiconductor lithography, and the necessary of increasing field size and throughput in displays. Although those difficulties may be common to the fabrication of DFB LDs, they would not be insurmountable problems. Even if defects in the imprinted pattern influence the yield of LDs, failed chips could be easily rejected because each dye is as small as approximately $300\ \mu\text{m}$. There is no need for a larger field size than a 3-in.-diameter circle, because the diameter of compound semiconductor substrates used for LDs is 3 inches or smaller. Regarding alignment accuracy, an error of up to approximately $5\ \mu\text{m}$ is acceptable. Even if throughput is limited to less than one wafer per hour, NIL would still have a higher throughput than EBL.

As described above, NIL is an effective and promising method for fabricating phase-shifted DFB LDs and is expected to have the advantage of mass-production capability in the near future. We conclude that NIL has high potential for fabricating DFB LDs, and we expect that NIL will be used for fabricating various optical devices consisting of nanostructures.

5. Acknowledgment

We would like to appreciate Dr. Taniguchi and his laboratory members at Tokyo University of Science for cooperative works and fruitful discussion.

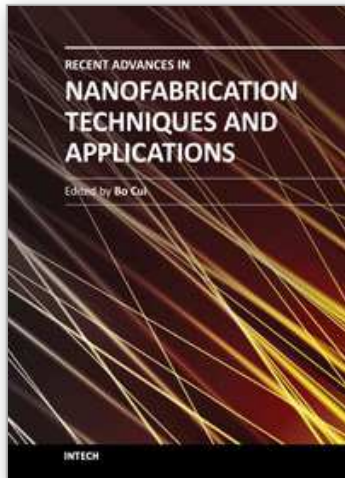
6. References

- Bailey, T.; Choi, B. J.; Colburn, M.; Meissl, M.; Shaya, S.; Ekerdt, J. G.; Sreenivasan, S. V. & Willson, C. G. (2000). Step and flash imprint lithography: Template surface treatment and defect analysis, *J. Vac. Sci. Technol.*, B 18, pp. 3572-3577, ISSN 1071-1023
- Chou, S. Y.; Krauss, P. R. & Renstrom, P. J. (1995). Imprint of sub-25 nm vias and trenches in polymers, *Appl. Phys. Lett.*, Vol. 67, pp. 3114-3116, ISSN 1077-3118
- Fukuda, M. & Iwane, G. (1985). Degradation of active region in InGaAsP/InP buried heterostructure lasers, *J. Appl. Phys.*, Vol. 58, pp. 2932-2936, ISSN 0021-8979
- Haisma, J.; Verheijen, M.; Heuvel, K. and Berg, J. (1996). Mold-assisted nanolithography: A process for reliable pattern replication, *J. Vac. Sci. Technol.*, B 14, pp. 4124-4128, ISSN 1071-1023
- Kaden, C.; Griesinger, U.; Schweitzer, H.; Pilkuhn, M. H. & Stath N. (1992). Fabrication of nonconventional distributed feedback lasers with variable grating periods and phase shifts by electron beam lithography, *J. Vac. Sci. Technol.*, B 10, pp. 2970-2973, ISSN 1071-1023
- Kinoshita, H.; Yamauchi, A. & Sawai, M. (1999). High-resolution resist etching for quartermicron lithography using O₂/N₂ supermagnetron plasma, *J. Vac. Sci. Technol.*, B 17, pp. 109-112, ISSN 1071-1023
- Kure, T.; Kawakami, H.; Tachi, S. & Enami, H. (1991). Low-Temperature Etching for Deep-Submicron Trilayer Resist, *Jpn. J. Appl. Phys.*, 30, pp. 1562-1566, ISSN 1347-4065
- Matsuoka, T.; Nagai, H.; Noguchi, Y.; Suzuki, Y. & Kawaguchi, Y. (1984). Effect of the grating phase at the cleaved facet on DFB laser properties, *Jpn. J. Appl. Phys.* 23, pp. L138-L140, ISSN 1347-4065
- Miller, M.; Doyle, G.; Stacey, N.; Xu, F.; Sreenivasan, S. V.; Watts, M. & LaBrake, D. L. (2005). Fabrication of nanometer sized features on non-flat substrates using a nano-imprint lithography process, *Proc. SPIE 5751*, pp. 994-1002
- Tsuji, Y.; Yanagisawa, M.; Yoshinaga, H.; Inoue, N. & Nomaguchi, T. (2011). Highly uniform fabrication of diffraction gratings for distributed feedback laser diodes by nanoimprint lithography, *Jpn. J. Appl. Phys.* 50, 06GK06, ISSN 1347-4065
- Yanagisawa, M.; Tsuji, Y.; Yoshinaga, H.; Kono, N. & Hiratsuka, K. (2009). Application of Nanoimprint Lithography to Fabrication of Distributed Feedback Laser Diodes, *Jpn. J. Appl. Phys.*, Vol. 48, 06FH11, ISSN 1347-4065

- Yanagisawa, M.; Tsuji, Y.; Yoshinaga, H.; Kono, N. & Hiratsuka, K. (2009). Evaluation of nanoimprint lithography as a fabrication process of phase-shifted diffraction gratings of distributed feedback laser diodes, *J. Vac. Sci. Technol.*, B 27, pp. 2776-2780, ISSN 1071-1023
- Yanagisawa, M.; Tsuji, Y.; Yoshinaga, H.; Kouno, N. & Hiratsuka, K. (2011). Wafer-level fabrication of distributed feedback laser diodes by utilizing UV nanoimprint lithography, *Proc. SPIE*, 7970, pp. 797014, ISSN 0277-786X

IntechOpen

IntechOpen



Recent Advances in Nanofabrication Techniques and Applications

Edited by Prof. Bo Cui

ISBN 978-953-307-602-7

Hard cover, 614 pages

Publisher InTech

Published online 02, December, 2011

Published in print edition December, 2011

Nanotechnology has experienced a rapid growth in the past decade, largely owing to the rapid advances in nanofabrication techniques employed to fabricate nano-devices. Nanofabrication can be divided into two categories: "bottom up" approach using chemical synthesis or self assembly, and "top down" approach using nanolithography, thin film deposition and etching techniques. Both topics are covered, though with a focus on the second category. This book contains twenty nine chapters and aims to provide the fundamentals and recent advances of nanofabrication techniques, as well as its device applications. Most chapters focus on in-depth studies of a particular research field, and are thus targeted for researchers, though some chapters focus on the basics of lithographic techniques accessible for upper year undergraduate students. Divided into five parts, this book covers electron beam, focused ion beam, nanoimprint, deep and extreme UV, X-ray, scanning probe, interference, two-photon, and nanosphere lithography.

How to reference

In order to correctly reference this scholarly work, feel free to copy and paste the following:

Masaki Yanagisawa (2011). Application of Nanoimprint Lithography to Distributed Feedback Laser Diodes, Recent Advances in Nanofabrication Techniques and Applications, Prof. Bo Cui (Ed.), ISBN: 978-953-307-602-7, InTech, Available from: <http://www.intechopen.com/books/recent-advances-in-nanofabrication-techniques-and-applications/application-of-nanoimprint-lithography-to-distributed-feedback-laser-diodes>

INTECH
open science | open minds

InTech Europe

University Campus STeP Ri
Slavka Krautzeka 83/A
51000 Rijeka, Croatia
Phone: +385 (51) 770 447
Fax: +385 (51) 686 166
www.intechopen.com

InTech China

Unit 405, Office Block, Hotel Equatorial Shanghai
No.65, Yan An Road (West), Shanghai, 200040, China
中国上海市延安西路65号上海国际贵都大饭店办公楼405单元
Phone: +86-21-62489820
Fax: +86-21-62489821

© 2011 The Author(s). Licensee IntechOpen. This is an open access article distributed under the terms of the [Creative Commons Attribution 3.0 License](#), which permits unrestricted use, distribution, and reproduction in any medium, provided the original work is properly cited.

IntechOpen

IntechOpen